Numerical simulation of angular injection of hydrogen fuel in scramjet combustor

M S R Chandra Murty[1] and **D Chakraborty**[2*]
Directorate of Computational Dynamics, Defence Research and Development Laboratory, Hyderabad, India

The manuscript was received on 16 December 2010 and was accepted after revision for publication on 31 May 2011.

DOI: 10.1177/0954410011414320

Abstract: Angular injection of hydrogen fuel in a scramjet combustor is explored numerically. Three-dimensional Navier–Stokes equations with turbulence and combustion models are solved using commercial computational fluid dynamics software. Both infinitely fast kinetics and single-step finite rate H_2–air kinetics are used to find out the effect of chemical kinetics in the thermo-chemical behaviour of the flow field. Grid independence of the results is demonstrated and grid convergence index-based error estimate provided. k-ω turbulence model performs better, in comparison to k–ϵ and shear stress transport models, in predicting the surface pressure. Single-step finite rate chemistry (SSC) performs extremely well in predicting the flow features in the combustor. Computed temperature and species mole fraction and wall pressure distributions with SSC match better with the experimental results compared to fast chemistry calculation and detailed chemistry calculation of other workers. It has been observed that simple chemistry can describe H_2–air reaction in scramjet combustor reasonably well.

Keywords: scramjet, CFD, fast chemistry, combustion model

1 INTRODUCTION

Sustained flight at hypersonic speed in the atmosphere remains the largest unexplored region of the possible flight envelope. Development of air-breathing hypersonic technology has been the subject of renewed interest since the 1980s because of tremendous military and commercial opportunities. The success of efficient design of such a transatmospheric hypersonic vehicle depends largely on the proper choice of the propulsion system which is capable of producing large thrust to overcome the drag experienced by the vehicle. These type of vehicles, according to current proposals, use supersonic combustion Ramjet (scramjet) propulsion system.

The development of efficient scramjet engine requires a detailed understanding of the complex mixing and combustion process inside the combustor. The flowfield inside the scramjet combustor is fully three-dimensional with strong shock boundary layer interaction. The diffusive mode of combustion in which energy is added gradually is preferred over the premixed mode in the scramjet combustor to minimize the intake–combustor interaction. The flowfield inside the combustor is very complex where fluid dynamics and chemistry interact very strongly.

Starting from pioneering work of Ferri [**1**], enormous amount of flow investigations have been performed in various countries on different aspects of scramjet flow field including ignition, flame holding, fuel injection, and intake combustor interaction. Both hydrogen and kerosene fuel have been considered. Although hydrogen has significant features in terms of ignition and specific impulse, high specific density and handling issues have rendered hydrocarbon as an attracted fuel for volume-limited application in the lower range ($M < 8$) of scramjet-operating envelope. In a recent review, Curran [**2**] has identified two emerging scramjet applications namely (1)

*Corresponding author: Directorate of Computational Dynamics, Defence Research and Development Laboratory, Kanchanbagh, Hyderabad 500058, India.
email: debasis_cfd@drdl.drdo.in

hydrogen-fuelled engine to access space and (2) hydrocarbon-fuelled engines for air-launched missiles. Considerable efforts have been focused on different injection schemes like cavity, strut, and pylon for different geometrical configurations and flow conditions in the past two decades. Selected methods that have been used to enhance the mixing process in the scramjet engines are summarized and reported in reference [**3**].

With the advent of powerful computer, robust numerical algorithm, computational fluid dynamics (CFD) complements 'difficult to perform' experiment and plays a very major role in the development of scramjet combustor through analysis of various thermochemical parameters obtained from the numerical simulation. Supersonic combustion with hydrogen fuel has been studied extensively both experimentally [**4–7**] and numerically [**8–13**] in the literature. These studies mostly measure and compare the wall properties (surface pressure and heat flux) and exit profiles for various flow parameters. Detailed diagnostics of flow distribution, namely temperature and species mass fraction across a cross-section inside the combustor, is very limited. Recently, to validate CFD data, a scramjet model known as SCHOLAR has been tested at NASA Langley's Direct Connect Supersonic Test facilities [**14, 15**]. Hydrogen fuel is injected at 30° angle to Mach 2 airstreams with 1200 K temperature in a divergent duct. Detailed measurement of temperatures at various cross-sections using coherent anti-Stokes Raman spectroscopy (CARS) thermometer and wall pressures are used to understand the progress of mixing and reaction in the combustor. The notable features of the experiments are: (1) flow field contains relevant features of high-speed engine flow path such as supersonic mixing and combustion with embedded regions of subsonic and recirculating flow, (2) geometry is simple so that proper interpretation of data is possible, (3) experiments have well-defined and well-controlled inflow and boundary conditions and well-quantified uncertainties, and (4) adequate measurements of surface pressure, surface temperature, species concentration, and temperatures at various cross-sectional planes enable detail comparisons of flow variables.

The SCHOLAR experiment has been simulated extensively using NASA Langley's VULCAN CFD code [**16**]. VULCAN (viscous upwind algorithm for complex flow analysis) is a cell-centred finite-volume, structured grid, multi-block code which solves the calorically perfect gas or of an arbitrary mixture of thermally perfect gases undergoing non-equilibrium chemical reactions. The inviscid fluxes are computed using the MUSCL scheme with either the approximate Riemann solver of Roe or the low dissipation flux splitting scheme of Edwards. The viscous fluxes can be evaluated either with or without cross-derivative contributions. It has a wide array of space and time integration schemes as well as thermodynamic, chemistry, and number of two-equation turbulence models. A detailed description of VULCAN code is available in reference [**16**]. Cutler *et al.*, [**17**] and Rodrigues and Cutler [**18**] have used k–ω turbulence model with various constant values of Pr_t and Sc_t. H_2–air reaction mechanism is modelled using Drumnond's 9 species 18-reaction mechanism [**19**] H_2–air kinetics. The computed results were seen to vary greatly with the specification of Pr_t and Sc_t. Recently, Keistler [**20**] adopted closure equations [**21, 22**] for turbulent Schmidt number and turbulent Prandtl number alongwith k–ω turbulence model [**23**] to study the same experiment. H_2–air chemical kinetic is modelled through seven species, seven reaction scheme due to Jachimowski [**24**] and the effects of turbulence–chemistry interaction model were investigated. It has been observed that with the addition of turbulence–chemistry interaction, there is a dramatic increase in the turbulent diffusivity throughout the flame region. With increase in computer power, large eddy simulations (LESs) are increasingly being attempted in simulating scramjet engine model [**25**]. Ingenito and Bruno [**26, 27**] have performed LES computations of the SCHOLAR experiment. The results were reasonable, but the grids used in all cases were quite coarse, even for a RANS simulation. It is clear that modelling issues in high-speed turbulent reactive flows need further investigation since higher order turbulence and chemical reaction models are computationally prohibitive for practical engineering application.

In this study, SCHOLAR experiment has been explored numerically using Fluent [**28**] commercial CFD software with standard turbulence model, simple chemical kinetic scheme, and simple turbulence–chemistry interaction model to find the capability of these standard physical and chemical models to predict the overall features of the mixing and reaction of high-speed turbulent reacting flow in a confined duct. Insight into the flow development process is obtained for parallel injection of hydrogen fuel into supersonic stream. Three-dimensional Navier–Stokes equations are solved using commercial CFD software. Effects of various turbulence models and chemical kinetics on the flow were studied. Computed thermo-chemical variables are compared with experimental and other numerical calculations [**17**].

2 DESCRIPTION OF TEST SET-UP AND THE COMBUSTOR FOR WHICH THE SIMULATION IS CARRIED OUT

The SCHOLAR experiment has been discussed extensively in the literature. Vitiated air corresponding to Mach 7 enthalpy is produced in a heater by combustion of Hydrogen with premixed oxygen and air. Oxygen is replenished so that the vitiated air at combustor entry will have oxygen mass fraction as that of pure air. The layout and dimensions of heater, injector nozzle set-up, and combustor model are shown in Fig. 1. The heater stagnation pressure is 0.765 $\pm$ 0.008 MPa and stagnation temperature (as estimated for one-dimensional (1D), inviscid, equilibrium chemistry analysis) 1827 $\pm$ 75 K. The total mass flowrate of heater is 1.2434 kg/s (air 0.915 kg/s, H_2 0.028 4 kg/s, and O_2 0.300 kg/s) with 3 per cent uncertainly in mass flowrate measurement. The high-pressure vitiated air is accelerated through a water-cooled Mach 2 nozzle before it enters the combustor entry test section. The nominal exit conditions of the nozzle are estimated from 1D analysis. The static temperature, static pressure, and Mach number at nozzle exit are 1187 $\pm$ 60 K, 0.1 $\pm$ 0.001 5 MPa, and 1.989 $\pm$ 0.005, respectively. All the uncertainties are due to mass flowrate measurement error and run-to-run variations in heater condition. Nozzle exit vitiated air is assumed to be composed of N_2, O_2, and H_2O with mass fractions 0.5638, 0.2321, and 0.2041, respectively.

The combustor duct consists of two constant area isolators that end in a step in the top wall. Downstream of the step there is another short constant area section followed by 3° divergence on the top wall up to the exit of the combustor. The length of the combustor is 1.45 m and the width (0.88 m) is constant throughout the combustor. The height of the combustor at entry is 38.86 mm while the height at the exit is 112 mm. The injection nozzle provides hydrogen fuel at 30° angle. The stagnation pressure, stagnation temperature, and exit Mach number of the injection nozzle are 3.44 $\pm$ 0.07 MPa, 302 $\pm$ 4 K, and 2.5, respectively. The mass flowrate of H_2 is 22.8 g/s resulting in equivalence ratio 0.99 $\pm$ 0.04.

The forward section of the combustor is made of copper while the rearward portion (divergent section) is made of carbon steel. The wall thickness and thermal conductivity of the test section allow the combustor to run without cooling. Wall pressures are measured at location at the top, bottom, and side walls while the temperatures are measured at three locations in the top wall only. To enable the measurement of temperature field by CARS beam, few transverse slots are provided in the combustor (mark 1, 3, 5, 6, 7) at distances 121.8, 274.2, 426.6, 777.0, and 1234.2 mm from the combustor entry.

3 COMPUTATIONAL METHODOLOGY

Simulations are carried out using a commercial CFD software Fluent [**28**]. It solves three-dimensional

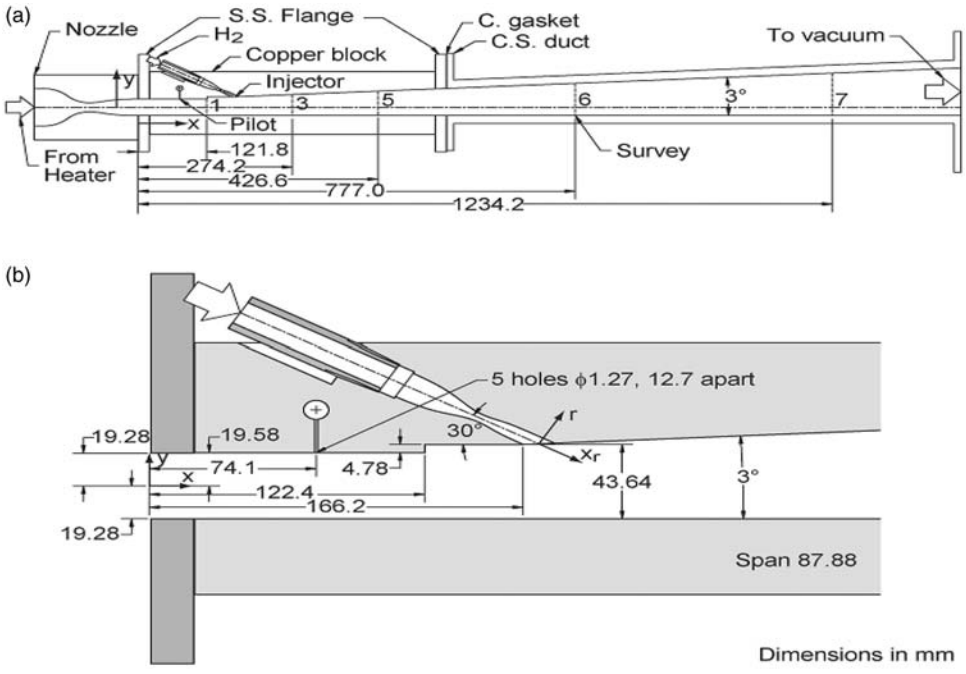

Fig. 1 Schematic of scholar experiment: (a) nozzle and combustor and (b) exploded view near fuel injector

Navier–Stokes equation in a structured, multiblock grid system using a collocated variable arrangement. To simulate high-Mach number compressible flow (as in the present case), a density-based solver is used alongwith second-order accurate Roe flux difference splitting scheme [**29**] for spatial discretization and first-order implicit Euler scheme for temporal discretization. Various turbulence models namely, k–ε, k–ω, and Menter's shear stress transport (SST) models, were studied to compare their predictive capability in turbulent reacting flows.

The chemistry of hydrogen–air combustion reaction is represented on a molar basis by $H_2 + 0.5O_2 = H_2O$. The mixing rate determined from the eddy dissipation model (EDM) is given as:

$$R_{k,\mathrm{edm}} = -A_{\mathrm{ebu}}\rho\frac{\varepsilon}{K}\min\left\{Y_{\mathrm{f}},\ \frac{Y_{\mathrm{o}}}{r_k},\ B_{\mathrm{ebu}}\frac{Y_{\mathrm{p}}}{1+r_k}\right\} \tag{1}$$

where ρ, Y_{f}, Y_{o}, and Y_{p} are the density and mass fractions of fuel, oxidizer, and products, respectively, A_{ebu} and B_{ebu} the model constants, and r_k the stoichiometric ratio.

In the single-step finite rate chemistry (SSC), the following reversible reaction involving H_2, O_2, and H_2O is considered.

$$2H_2 + O_2 \Leftrightarrow 2H_2O$$

and the net rate of reaction of H_2 (in kg-mol/m^3 s) is given by the expression [**30–32**]

$$\frac{\mathrm{d}C_{\mathrm{H_2}}}{\mathrm{d}t} = -2\left[1.102\times10^{19}\exp\left(\frac{-8052}{T}\right)C_{\mathrm{H_2}}^2 C_{\mathrm{O_2}} - k_b C_{\mathrm{H_2O}}^2\right] \tag{2}$$

where c is the molar concentration (in g-mol/cm^3) and k_b the rate constant of the reverse reaction, is obtained from the forward rate constant and equilibrium constant.

The eddy dissipative concept (EDC) set forth by Magnussen and Hjertager [**33**] gives an empirical expression for the mean reaction rate based on the assumption that chemical reaction occurs in an isolated region where the dissipation of turbulent energy is significant. Recently, Gran *et al.* [**34, 35**] gave the formulation for reaction rates for finite rate chemistry based on the EDC. Following Gran, the mean reaction rate for the species i (w_i) is given by

$$\frac{\bar{w}_i}{\rho} = \frac{\gamma^2\chi}{\tau^*}\left(Y_i^0 - Y_i^*\right) \tag{3}$$

where χ is the fraction of the fine structures where reaction occurs and superscripts '0' and '*' the surrounding fluids and fine structure region; τ^* the time scale for the mass transfer between the fine structures and the surroundings. The fine structure is considered as a constant pressure homogeneous reactor where all the properties are time dependent and no spatial gradient exists. The set of governing equation for such a reactor is

$$\frac{\mathrm{d}h}{\mathrm{d}t} = 0 \tag{4}$$

$$\frac{\mathrm{d}p}{\mathrm{d}t} = 0 \tag{5}$$

$$\frac{\mathrm{d}Y_i}{\mathrm{d}t} = \frac{w_i}{\rho} + \nu_\gamma\left(Y_i^m - Y_i^0\right) \tag{6}$$

where the superscript m refers to the fluid entering the reactor and ν_r the rate of mixing. The equation [**6**] is integrated from $t = t_0$ to $t = t_0 + \Delta t$. The reactor type is determined by the choice of ν_r and Δt in equation (6). Magnussen and Hjertager [**33**] assumed that the reactors are stationary with mixing rate $\nu_\gamma = 1/\tau^*$. This corresponds to a perfectly stirred reactor with residence time τ^*. The steady state is obtained by taking the limits $\Delta t \to \infty$. A more detailed description of the EDC-based finite rate combustion model is available in reference [**36**].

Chakraborty *et al.* [**37**] has carried out direct numerical simulation (DNS) of H_2–air mixing layer of Erdos experimental case [**6**] and investigated the effect of fast chemistry (FC), single-step chemistry, and seven species seven reaction finite rate chemistry in the thermochemical behaviour of reacting mixing layer. The computed DNS database was used to evaluate the existing combustion models [**36**]. It was shown that finite rate EDC-based combustion model could predict the overall trend of reaction rate profiles although the model predicts a thin reaction zone compared to DNS data.

Finite rate calculations are performed with the help of Chemkin software. A coupling code is written to make calls between Chemkin and Fluent. At every time step δt, the current solution field are taken from Fluent solver including mass fraction of every species, temperature, and pressure. These values are used as initial conditions for Chemkin solver. Chemkin solves the reaction rates for each species and estimates the mass fractions of all species and temperature and transfers these values to Fluent solver. This process continues for every iteration of Fluent solver.

4 RESULTS AND DISCUSSION

The computational domain of the total set-up is divided into two parts, namely facility nozzle and combustor with fuel injection system. These flow fields are simulated sequentially and the solution at the exit plane of the facility nozzle provides values of various flow variables at combustor entry plane.

A number of reacting simulations were carried out in the combustor by varying grid, turbulence model, chemical kinetics, and equivalence ratios so that the effects of each of one these factors can be estimated. A reference base line solution was first found out based on k–ω turbulence model and EDC-based infinitely fast rate kinetics and equivalence ratio 1.0. Parametric studies were carried out on this baseline solution.

Taking advantage of the geometrical symmetry, only half width of the combustor is simulated. In the simulation, x-axis is taken along width of the combustor, while y- and z-axes are along the height and length of the combustor, respectively. The origin is placed at combustor inflow centre. Simulations were carried out for two different grids, namely (1) $30 \times 65 \times 415$ (2) $30 \times 26 \times 250$. Grids in the longitudinal and vertical directions have been varied. A typical computational grid in the combustor is shown in Fig. 2. Injector geometry is simulated and appropriate hexahedral grid taken in the injector region. Inflow condition at the inlet of the hydrogen injector is assumed subsonic and stagnation pressure of 3.44 MPa and stagnation temperature 302 K are specified at the inflow plane of the injector. The nozzle provided H_2 to the combustor chamber at 30° angle. The exit Mach number of the H_2 injection nozzle is 2.5.

For steady-state boundary-value problem, the main source of numerical error in CFD is iterative convergence or grid convergence error [**38**]. Grid convergence or discretization error, which is the error of the solution of the difference equations compared to the exact solution of the partial differential equation, is the major source of numerical error. This error can be estimated by running the solution in two different grids (coarse and fine). The simplest of such estimate is given by the relative difference $\varepsilon = (f_2 - f_1)/f_1$ [**17**], where f represents any quantity of interest and the indices 1 and 2 the fine and coarse grid solutions, respectively. Roache [**39**] has proposed a grid-convergence index (GCI) as an error based on uncertainty estimate of the numerical solution as

$$\mathrm{GCI} = F_\mathrm{s} \frac{1\varepsilon 1}{(h_2/h_1)^p - 1} \tag{7}$$

where h is the order of grid spacing, p the order of accuracy of numerical scheme and, F_s a factor of safety. Roache [**40**] has suggested $F_\mathrm{s} = 3$ for minimal of two grid calculations. For the present calculation, p is equal 2 with h_2/h_1 equal to 4.15, and GCI is of the order 0.2ϵ. The axial distribution of computed surface pressure on the top wall is presented in Fig. 3. After the fuel injection at $x = 0.2$ m, the flow is getting disturbed significantly due to injection and reactions resulting in a number of shock reflections between up to $x = 0.8$ m. In the divergent portion of the combustor, flow becomes smooth. It can be observed that by changing the grids to nearly four times, the results do not change much. The axial distribution of the computed percentage error estimate is also presented in the same figure. However, for the injection location, maximum error between two simulations is within 5 per cent. This analysis indicates that the

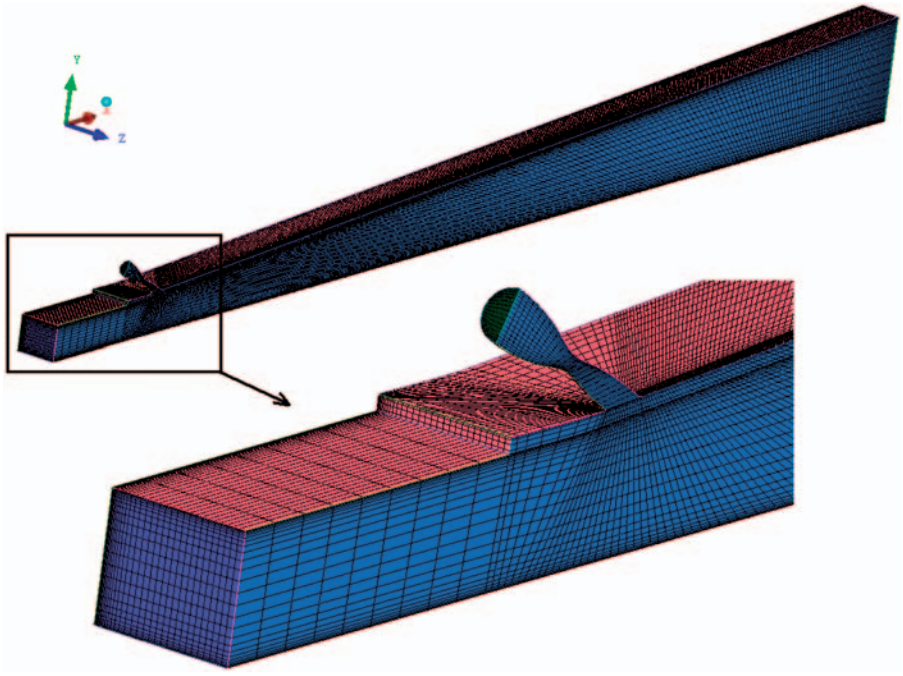

Fig. 2 Computational grid in the combustor

baseline grid is adequate to capture most of the features of the flow and the solution is grid independent.

Cross-sectional views of Mach number distributions at various axial planes are shown in Fig. 4. Significant reduction of Mach number is seen to occur due to reaction in upper portion of the combustor. Flow remains mostly supersonic throughout the combustor, indicating the prevalence of supersonic combustion in the combustor. The cross-sectional non-uniformity of the flow exists only near the station 3 ($x = 0.2$ m). To illustrate the point more clearly, the axial distribution of surface pressure at the centre-line of top wall, bottom wall, and side walls are plotted in Fig. 5. Significant difference of surface pressure between the three walls is observed only up to $x = 0.4$ m, indicating that three-dimensionality of the flow is existing in the near-field region of injection. Hydrogen and oxygen mass fraction contours at symmetry plane are presented in Fig. 6. Although, small trace of hydrogen mass fraction is seen up to the end of the combustor, oxygen is seen to be consumed totally.

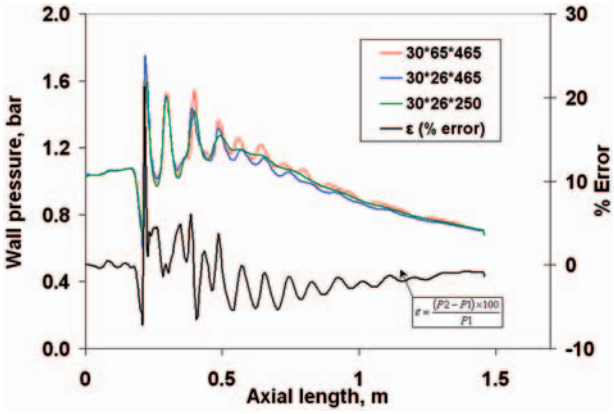

Fig. 3 Axial distribution of wall pressure and error estimate for two grids

To find out the region of premixed and diffusion-dominated combustion, the distribution of the term $\Delta Y_{H_2} \cdot \Delta Y_{O_2}$ in the symmetry plane is presented in Fig. 7. Yamashita *et al.* [**41**] used this index to determine the zone of premixed and diffusion combustion in the mixing layer. The basic idea is that if the dot product of the gradient of fuel and oxidizer mass fraction is strongly negative, then the zone is dominated by diffusive combustion since the flame are fed by the oxidizer and fuel from opposite direction; if the quantity is strongly positive, the zone is affected by premixed combustion since the fuel and oxidizer is fed from the same side. From the figure, it is clear that near the injection and mixing zones, burning is mostly diffusive in nature and small region of premixed combustion is seen in the upper portion of the combustor.

The velocity profile in the symmetry plane at $x = 1.234$ m (station 7) is compared between no reaction (NR), FC, and SSC in Fig. 8. It can be observed that velocity profile for NR case is similar to that of FC calculation, while the velocity profile with SSC is marginally different. This demonstrates that the effect of gas dynamics is predominant and the change of enthalpy due to chemistry is not large compared to the total enthalpy. The temperature and water mass fraction profiles at station 7 are compared for the FC and SSC calculations in Fig. 9. The temperature profile for NR case is also plotted in the figure. Significant variation of temperature profile is observed because of reaction. FC calculation shows the maximum temperature because of absence of heat-absorbing reaction path. Water mass fraction profile is similar to that of temperature profile because of assumption of unity Lewis number. It is seen that while velocity changes are effected by gas dynamics, the change in the temperature and water mass fraction is related to the chemical reactions.

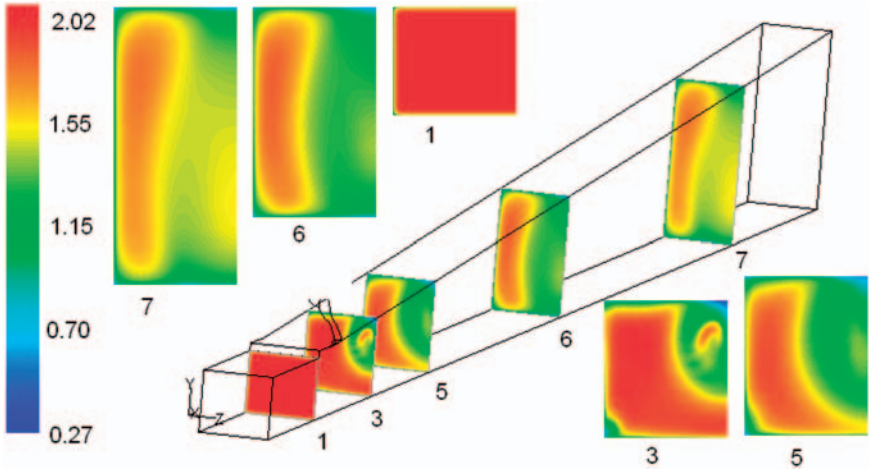

Fig. 4 Cross-sectional view of Mach number distribution of reacting case

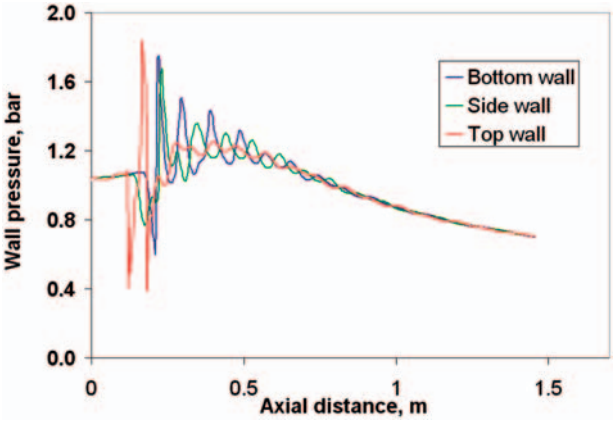

Fig. 5 Axial distribution of surface pressure at top wall bottom wall and side wall

4.1 Effect of turbulence model

Three different turbulence models namely k–ω, k–ε, and SST have been employed to study their effect in the combustor flow field. The axial distribution of computed surface pressure with different turbulence model is presented in Fig. 10. The predicted surface pressures for all three turbulence models are higher in the injection zone because of FC assumption. In the divergent portion of the combustor, k–ω performs extremely well. k–ε predicts slightly higher surface pressure near the exit of the combustor. The performance of SST turbulence model is the poorest among the three. The predicted surface pressure is quite lower compared to the experimental value.

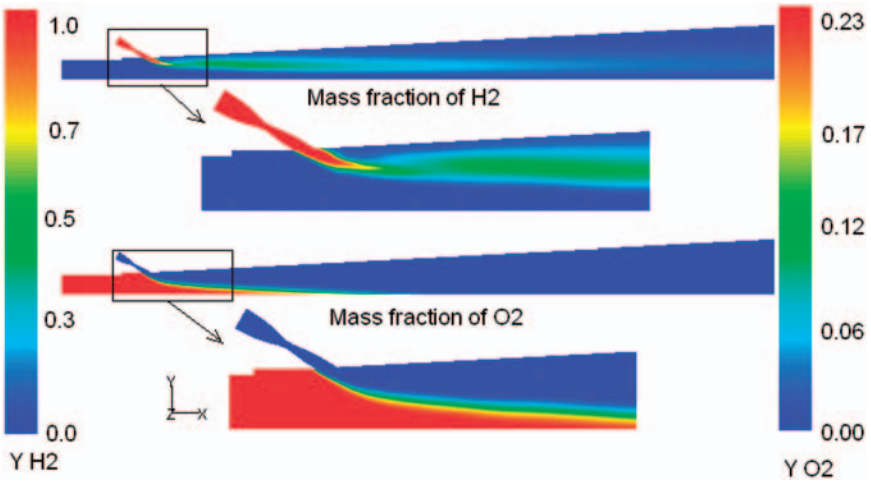

Fig. 6 Hydrogen and oxygen mass fraction contours at the plane of symmetry

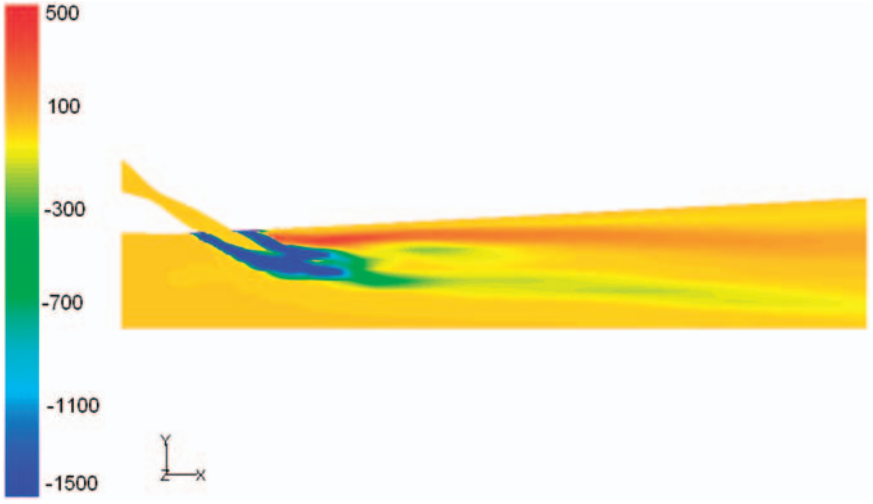

Fig. 7 Distribution of $\Delta Y_{H_2} \cdot \Delta Y_{O_2}$ at injection region

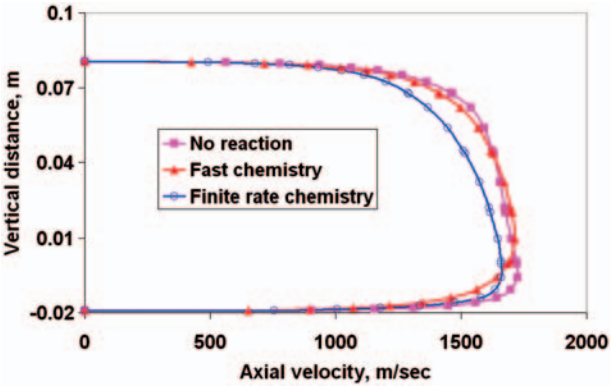

Fig. 8 Velocity profile at $X = 1.234$ m (Plane-7)

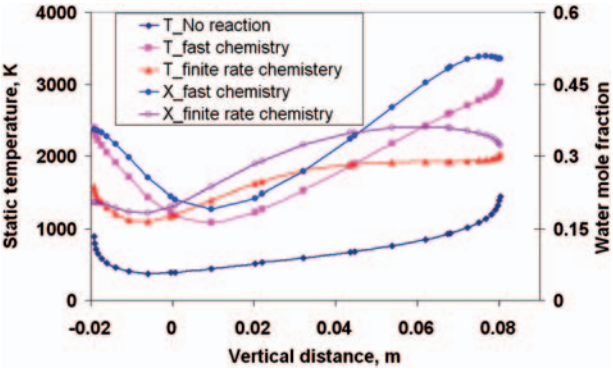

Fig. 9 Variation of static temperature and water mole fraction at Plane-7

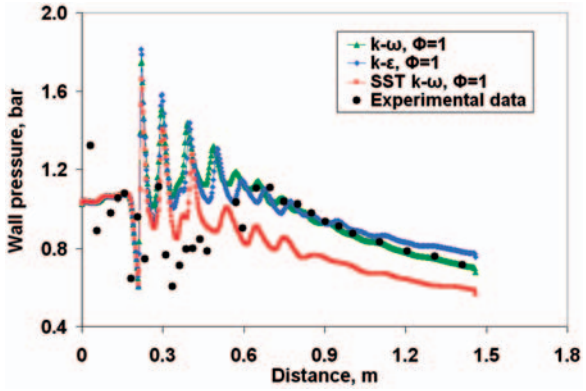

Fig. 10 Comparison of combustor top wall surface pressure with different turbulence models

4.2 Effect of equivalence ratio

Parametric studies are carried out for different equivalence ratios, namely $\phi = 1.0$, 0.7, and 0.5. The axial distributions of computed surface pressure with different equivalence ratios are compared in Fig. 11. The computed surface pressures for the case without fuel injection and for the case with fuel injection but NR (mixing) cases are also plotted in the figure. Throughout the combustor, the surface pressure for

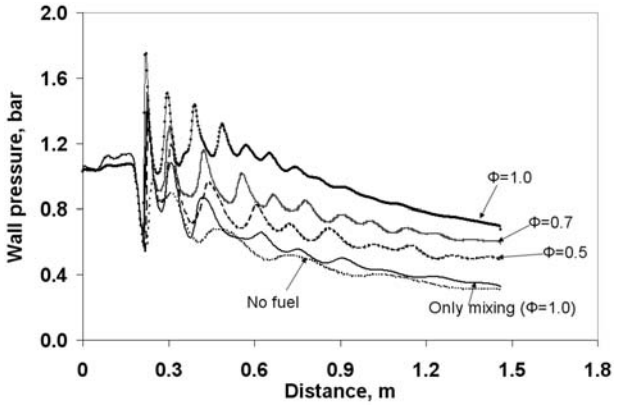

Fig. 11 Comparison of combustor top wall surface pressure with different equivalence ratios

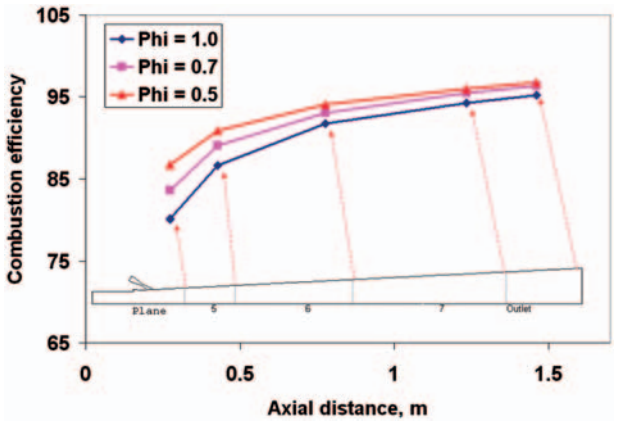

Fig. 12 Axial distribution of combustion efficiencies for different equivalence ratios

the reacting case is significantly higher than the non-reacting case. The difference between non-reacting and reacting surface pressures is responsible for getting the thrust in the combustor. The computed thrust and the combustion efficiency at the exit are tabulated in Table 1. The thrust of the combustor is defined as the difference of the outflow and inflow momentums The axial distribution of combustion efficiency for different equivalence ratios is presented in Fig. 12. Following Kim *et al.* [**42**], combustion efficiency is defined as

$$\eta_c(x) = 1 - \frac{\int \rho u y_F \mathrm{d}A}{(\rho u y_F \mathrm{d}A)_{x=0}} \tag{5}$$

where y_F and m_F are the mass fraction and mass flow-rate of hydrogen fuel.

The maximum combustion efficiency for $\phi = 1.0$ is about 95 per cent. Hence, the reaction has almost gone to completion. For lower equivalence ratios, the combustion efficiency is still higher. As expected, computed thrust increases with increase in equivalence ratio.

Table 1. Computed thrust and maximum combustion efficiency

Equivalence ratio	Thrust (N)	Combustion efficiency (%) at the exit
1.0	465.08	95.15
0.7	424.38	96.35
0.5	393.60	96.70

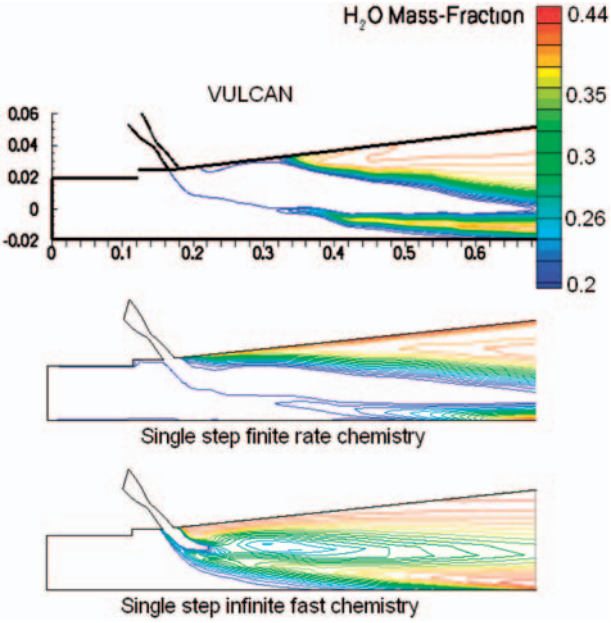

Fig. 13 Comparison of H_2O mass fraction with VULCAN code at plane of symmetry

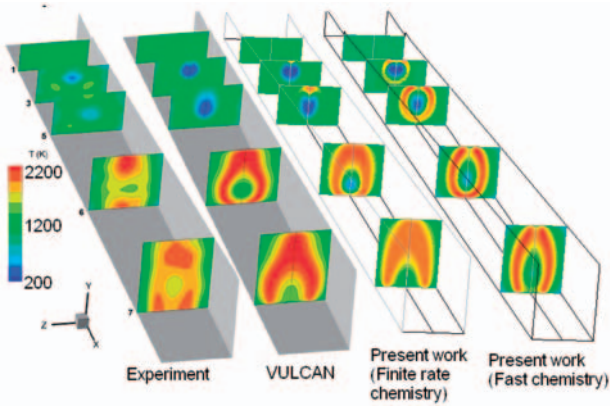

Fig. 14 Comparison of temperature distribution at various cross-sections between experiment, VULCAN, SSC, and fast-rate kinetics

4.3 Effect of chemical kinetics

Baseline solution predicted more surface pressure compared to the experimental pressure in the near-injection field. Instantaneous heat release caused due to the infinitely FC assumption in the analysis is conjectured to be reason of higher surface pressure. Effect of finite rate chemistry is investigated by carrying out simulations with single-step finite rate chemical kinetics for H_2–air system. In the single-step H_2–air finite rate chemistry, the reversible reaction $2H_2 + O_2 \Leftrightarrow 2H_2O$ involving H_2,O_2, and H_2O is considered. Details of chemical kinetics and turbulence–chemistry interaction employed in the study are explained in section 3. H_2O mass fraction contour at the plane of symmetry is compared with VULCAN simulation results [**18**] in Fig. 13. The zone of water mass fraction contour is more in the present computation compared to the VULCAN results. It is to be noted that VULCAN used Drumnond's 9 species 18-reaction mechanism [**19**] for H_2–air kinetics without any modelling of turbulence–chemistry interaction, whereas in the present computation, an infinitely FC and SSC with EDC turbulence–chemistry interaction model for finite rate chemistry [**33, 34**] is used. In the FC computation, reactions are comparatively fast. The formation of water mass fraction with the finite rate chemistry is reduced significantly compared to the FC. The computed water mass fraction with SSC matches reasonably well with the 9 species 18 reaction model of VULCAN. This result suggests that a simpler chemistry may be adequate to explain the combustion of H_2 in the scramjet combustor if a proper turbulence–chemistry interaction model is used. Temperature contours at different cross-sectional planes are compared with experiment and VULCAN results in Fig. 14. Results for the baseline configuration are also presented in the figure to see the effect of chemical kinetics. Although qualitative features of experimental temperature distribution have been captured in the numerical simulations, finer details of the reacting flow field differ between the experiment and computation. Diffusion is seen to be more in the experimental condition compared to the numerical calculation. Whether calculation with varying turbulent Schmidt number can resolve this difference is not known. Mole fraction contours of O_2 and N_2 at different cross-sections are compared with experimental results, VULCAN, and FC results in Figs 15 and 16, respectively. Present computation with finite rate chemistry compares the experimental features of the reacting flow field better than the other numerical simulations.

Computed surface pressure for SSC is compared with baseline results, experimental data, and the VULCAN results [**18**] in Fig. 17. In the figure, it is clearly seen that in the injection and reaction zone prediction methodologies differ from each other and also with the experimental results, whereas in the divergent section of the combustor ($x > 0.8$ m), where majority of thrust is produced, all the

methodologies match with the experimental results. In the injection and reaction zones, FC calculation shows the highest surface pressure. As expected, instantaneous heat release assumed in the analysis makes the surface pressure maximum. SSC performs very well in predicting the surface pressure throughout the combustor. In the near-injection field, the computed results of SSC match with the experimental results better. The computation also captures various shock reflections found in the experimental results. Computed pressure distribution in the symmetry plane presented in Fig. 18 shows intense shock reflections in the downstream of the injection point. As one proceeds downstream, due to increase in combustor area, the flow undergoes expansion and shock reflections disappear. The location of shock reflection points is slightly different from the experimental value. Pressure levels with finite rate chemistry are significantly lower compared to the FC results. Introduction of backward reaction (which is endothermic) reduces the net heat release and thus the pressure rise. In the zone between 0.6 to 0.8 m, the SSC predicts lesser pressure compared to the experimental values. One can observe the presence of two strong shock reflections in VULCAN result in the region between 0.5 to 0.6 m. These strong shocks were not observed in experimental results and

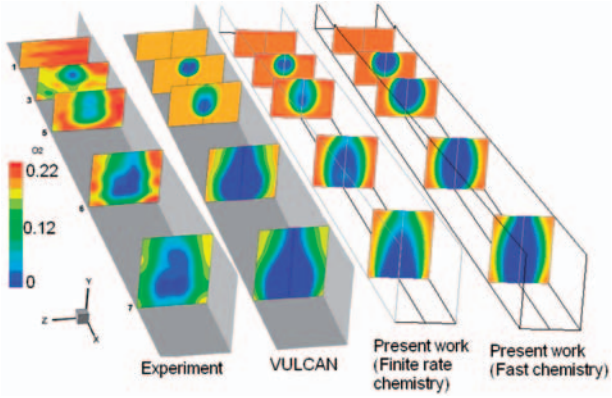

Fig. 15 Comparison of O_2 mole fraction distribution at various cross-sections between experiment, VULCAN, SSC, and fast-rate kinetics

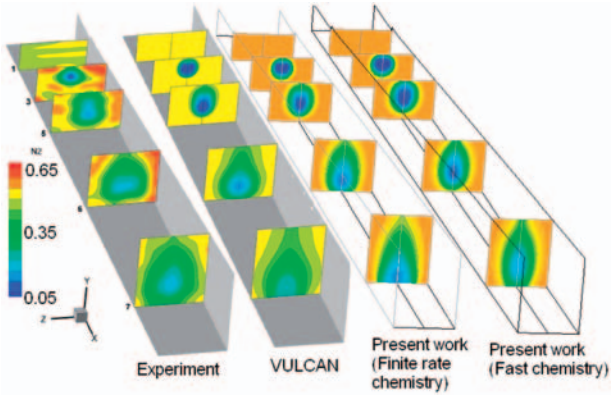

Fig. 16 Comparison of N_2 mole fraction distribution at various cross-sections between experiment, VULCAN, SSC, and fast-rate kinetics

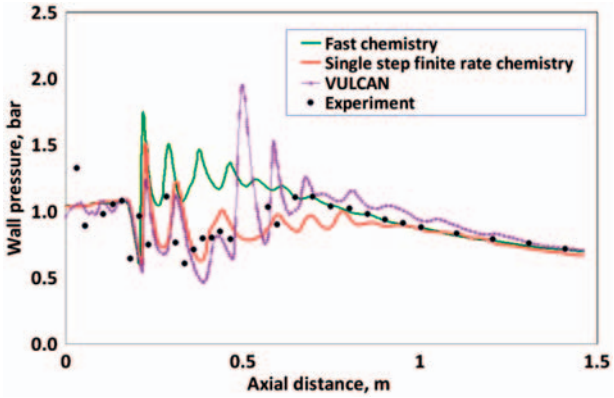

Fig. 17 Surface pressure comparison between experimental data, finite rate chemistry, FC, and VULCAN result

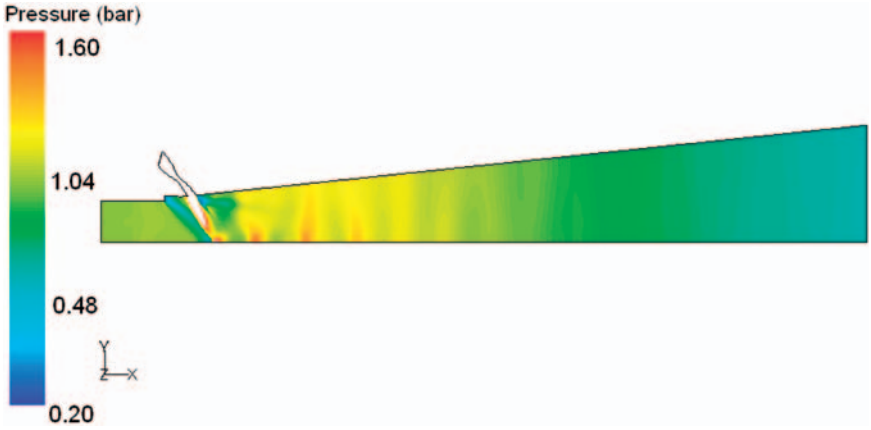

Fig. 18 Pressure distribution in symmetry plane along axial direction

present computations and the reasons for their occurrence are not very clear. In the downstream region of combustor ($X > 0.6$), VULCAN results show higher pressure values compared to the experiment, whereas the present computations (both FC and finite rate chemistry) match better with the experimental result due to a better grid distribution employed in the present simulation. The computed results indicate that single-step finite rate chemical kinetics with simple turbulence–chemistry interaction model is adequate to describe H_2–air reaction in the scramjet combustor.

5 CONCLUSIONS

The flow field of scramjet combustor with angular injection of hydrogen fuel is simulated numerically. Three-dimensional Navier–Stokes equations are solved in multiblock structured grid using commercial CFD software. Different turbulence models are used to find their predictive capability of turbulent reacting flows. H_2–air chemical reaction is modelled by employing two different chemical kinetics, namely infinitely fast rate kinetics and SSC and thermochemical behaviour of the flow field between the two are compared. EDC-based finite rate combustion model is employed to describe turbulence chemistry interaction. Grid independence of the solution is established and an error estimate in terms of grid convergence index has been provided. Simulation captures all the essential features of the flow field. k–ω turbulence model performs the best among the turbulence model tested. It has been observed that FC predicts more intensive and instantaneous reactions resulting in more surface pressure. SSC with EDC-based turbulence–chemistry interaction model performs extremely well in predicting the overall mixing and combustion process in the combustor. Computed temperature, species mole fraction distribution, and wall pressures with SSC match better with experimental results than the infinitely fast kinetics and detailed chemistry calculation of other researchers. The results indicate that simple chemical kinetics with EDC-based turbulence–chemistry interaction model is adequate to describe the H_2–air reaction in the scramjet combustor.

REFERENCES

1 **Ferri, A.** Review of problems in application of Supersonic Combustion. *J. Royal Aeronaut. Soc.*, 1964, **68**(645), 575–597.

2 **Curran, E. T.** Scramjet engines: The first forty years. *J. Propul. Power*, 2001, **17**(6), 1138–1148.

3 **Seiner, J. M., Dash, S. M.,** and **Kenzakowski, D. C.** Historical survey on enhanced mixing in Scramjet engines. *J. Propul. Power*, 2001, **17**(6), 1273–1286.

4 **Burrows, M. C.** and **Kurkov, A. P.** Analytical and experimental study of supersonic combustion of hydrogen in vitiated air stream. NASA Report No. NASA-TMX-2828, 1973.

5 **Cheng, T., Wehrmeyer, J., Pitz, R., Jarrett Jr, O.,** and **Northam, G.** Finite rate chemistry effects in a Mach 2 reacting flow. AIAA Paper No. 91-2320, 1991.

6 **Erdos, J., Tamagno, J., Bakos, R.,** and **Trucco, R.** Experiments on shear layer mixing at hypervelocity conditions. AIAA Paper No. 1992-0628, 1992.

7 **Tomioka, S., Murakami, A., Kudo, K.,** and **Mitani, T.** Combustion tests of a staged supersonic combustor with a strut. *J. Propul. Power*, 2001, **17**(2), 293–300.

8 **Drummond, J. P.** Supersonic reacting internal flow field in numerical approaches in combustion modeling. In *Progress in aeronautics and astronautics*, Vol. 135 (Eds E. S. Oran, J. P. Borris), 1991, pp. 365–420 (AIAA).

9 **Carpenter, M. H.** Three dimensional computations of cross flow injection and combustion in a supersonic flow. AIAA Paper No. 89-1870, 1989.

10 **Uenishi, K., Rogers, R. C.,** and **Northam, G. B.** Three dimensional computation of transverse hydrogen jet combustion in a supersonic air stream. AIAA Paper No. 87-0089, 1987.

11 **Chitsomboon, T.** and **Northam, G. B.** Computational fluid dynamics prediction of the reacting flowfield inside a subscale scramjet combustor. *J. Propul. Power*, 1991, **7**(1), 44–48.

12 **Saha, S.** and **Chakraborty, D.** Reacting flow computation of staged supersonic combustor with strut injection. AIAA Paper No. 2006-3895, 2006.

13 **Kim, S. W.** Numerical investigation of chemical reaction – turbulence interaction in compressible shear layer. *Combust. Flame*, 1995, **101**, 197–208.

14 **Cutler, A. D., Danehy, P. M., Springer, R. R., DeLoach, R.,** and **Capriotti, D.P.** CARS thermometry in a supersonic combustor for CFD code validation. AIAA Paper No. 2002-0743, 2002.

15 **Cutler, A. D., Diskin, G. S., Danehy, P. M.,** and **Drummond, J. P.** Fundamental mixing and combustion experiments for propelled hypersonic flight. AIAA Paper No. 2002-3879, 2002.

16 **White, J. A.** and **Morrison, J. H.** A pseudo-temporal multi-grid relaxation scheme for solving the parabolized Navier Strokes equation. AIAA Paper No. 99-3360, 1999.

17 **Cutler, A. D., Danehy, P. M., O'Byrne, S.Rodrigues, C. G.,** and **Drummond, J. P.** Supersonic combustion experiment for CFD model development and validation. AIAA Paper No. 2004-266, 2004.

18 **Rodrigues, C. G.** and **Cutler, A. D.** Computational simulation of a supersonic-combustion benchmark experiment. AIAA Paper No. 2005-4424, 2005.

19 **Drummond, J. P.** A two-dimensional numerical simulation of supersonic, chemically reacting mixing layer, NASA TM – 4053, NASA, 1988.

20 Keistler, P. G. *A variable turbulent Prandtl and Schmidt number model study for scramjet applications.* PhD dissertation, Department of Mechanical and Aerospace Engineering, North Carolina State University, 2009.

21 Xiao, X., Edwards, J. R., Hassan, H. A., and **Gaffney, R. L.** Role of turbulent Prandtl number on heat flux at hypersonic mach numbers. AIAA Paper No. 2005-1098, 2005.

22 Xiao, X., Hassan, H. A., and **Baurle, R. A.** Modeling scramjet flows with variable turbulent Prandtl and Schmidt numbers. AIAA Paper 2006-0128, 2006.

23 Alexopoulos, G. A. and **Hassan, H. A.** A k-ζ (enstrophy) compressible turbulence model for mixing layers and wall bounded flows. AIAA Paper No. 1996-2039, 1996.

24 Jachimowski, C. J. An analytic study of the hydrogen-air reaction mechanism with application to scramjet combustion. NASA Technical Paper No. 2781, 1988.

25 Berglund, M. and **Fureby, C.** LES of supersonic combustion in a scramjet engine model. *Proc. Combust. Inst.*, **31**(2), 2497–2504.

26 Ingenito, A. and **Bruno, C.** LES of a supersonic combustor with variable turbulent Prandtl and Schmidt numbers. AIAA Paper No. 2008-0515, 2008.

27 Ingenito A. and **Bruno, C.** Reaction regime in supersonic flows. AIAA Paper No. 2009 – 0812, 2009.

28 Ansys Fluent 6.3 software users guide, http://www.fluentusers.com/fluent63/doc/ori/index.htm, Ansys Inc., 2006.

29 Roe, P. L. Characteristic based schemes for the Euler equations. *Annu. Rev. Fluid Mech.*, 1986, **18**, 337–365.

30 Drummond, J. P. and **Mukunda, H. S.** A Numerical Study of of mixing enhancement in supersonic reacting flow field, AIAA Paper No. 1988-3260, American Institute of Aeronautics and Astronautics, 1988.

31 Drummond, J. P. and **Carpenter, M. H.** Mixing and mixing enhancement in supersonic reacting flow fields in high speed flight propulsion systems. In *Progress in astronautics and aeronautics*, Vol. 137 (Eds S. N. B. Murthy, E. T. Curran), 1991, pp. 383–455 (AIAA).

32 Sekar, B. and **Mukunda, H. S.** A computational study of direct simulation of high speed mixing layers without and with chemical heat release. In Proceedings of the 23rd International Symposium on *Combustion*, Orlean, France, 22–27 July 1990, pp. 707–713 (The Combustion Institute, Pittsburgh, Pennsylvania).

33 Magnussen, B. F. and **Hjertager, B. H.** On mathematical modeling of turbulent combustion with special emphasis on soot formation and combustion. In Proceedings of the 16th International Symposium on *Combustion*, Cambridge, Massachusetts, 15–20 August 1976, pp. 719–729 (The Combustion Institute, Pittsburgh, Pennsylvania).

34 Gran, I. R., Melaaen, M. C., and **Magnussen, B. F.** Numerical simulation of local extinction effects in turbulent combustor flows of Methane and air. In Proceedings of the 25th International Symposium on *Combustion,* Irvine, California, 31 July–5 August 1994, pp. 1283–1291 (The Combustion Institute, Pittsburgh, Pennsylvania).

35 Gran, I. R., Erttesvag, I. S., and **Magnussen, B. F.** Influence of turbulence modeling on predictions of turbulent combustion. *AIAA J.*, 1997, **35**(1), 106–110.

36 Chakraborty, D., Paul, P. J., and **Mukunda, H. S.** Evaluation of empirical combustion models for high speed H_2/air confined mixing layer using DNS data. *Combust. Flame*, 2000, **121**(4), 195–209.

37 Chakraborty, D., Nagraja Upadhaya, H. V., Paul, P. J., and **Mukunda, H. S.** A thermo-chemical exploration of two dimensional reacting supersonic mixing layer. *Phys. Fluids*, 1997, **9**(11), 3513–3522.

38 AIAA Guide for the verification and validation of computational fluid dynamics simulations (G-077-1998e), AIAA, 1998.

39 Roache, P. J. *Verification and validation in computational science and engineering*, 1998 (Hermora Publishers, New Mexico).

40 Roache, P. J. Error bar for CFD. AIAA Paper No. 2003-0408, 2003.

41 Yamashita, H., Shimada, M., and **Takeno, T.** A numerical study of flame stability at transition point of diffusion flames. In Proceedings of the 26th Symposium (International) on *Combustion*, Naples, Italy, 28 July–2 August 1996, pp. 27–34 (The Combustion Institute, Pittsburgh, Pennsylvania).

42 Kim, J. H., Yoon, Y., Jeung, I. S., Hwanil, H., and **Choi, J. Y.** Numerical study of mixing enhancement by shock where in model scramjet engine. *AIAA J.*, 2003, **41**(6), 1074–1080.